OCCAM

OXFORD CENTRE FOR COLLABORATIVE APPLIED MATHEMATICS

Computational probabilistic quantification of pro-arrhythmic risk from scar and left-to-right heterogeneity in the human ventricles

by

Mikael Wallman
Alfonso Bueno-Orovio
Blanca Rodriguez

OCCAM Preprint Number 13/29

Computational Probabilistic Quantification of Pro-arrhythmic Risk from Scar and Left-to-right Heterogeneity in the Human Ventricles

Mikael Wallman[1,3], Alfonso Bueno-Orovio[2], Blanca Rodriguez[1]

[1] Department of Computer Science, University of Oxford, Oxford, UK
[2] Oxford Centre for Collaborative Applied Mathematics, University of Oxford, Oxford, UK
[3] Fraunhofer-Chalmers Centre, Göteborg, Sweden

Abstract

Both scar and left-to-right ventricular (LV/RV) differences in repolarization properties have been implicated as risk factors for lethal arrhythmias. As a possible mechanism for the initiation of re-entry, a recent study has indicated that LV/RV heterogeneities in action potential duration (APD) adaptation can cause a transient increase in APD dispersion following rate acceleration, promoting unidirectional block of conduction at the LV/RV junction. In the presence of an ischemic region and ectopic stimulation, a pathological dispersion in repolarization has been suggested to increase the risk of electrical re-entry. However, the exact location and timing of the ectopic activation play a crucial role in initiation of re-entry, and certain combinations may lead to re-entry even under normal LV/RV dispersion in repolarization. This suggests that the phenomenon needs to be investigated in a quantitative way. In this study we employ a computationally efficient, phenomenological model in order to investigate the pro-arrhythmic properties of a range of combinations of position and timing of an ectopic activation. This allows us to probabilistically study how increasing interventricular dispersion of repolarization increases arrhythmic risk. Results indicate that a larger LV/RV dispersion in repolarization allows ectopic beats to initiate re-entry during a significantly larger time window and from a greater number of locations compared to the case of smaller LV/RV dispersion.

1. Introduction

Ventricular heterogeneity in repolarization is one of the most important contributors to the electrophysiological substrate leading to the occurrence of lethal arrhythmias such as ventricular fibrillation [1]. A number of studies have demonstrated the complex spatio-temporal mechanisms that modulate ventricular heterogeneity in repolarization and pro-arrhythmic risk. Ventricular heterogeneity in repolarization and arrhythmic risk are known to increase with sudden changes in rate [2, 3], due to the highly rate-dependent properties of the APD. The dynamics of APD adaptation underlie the adaptation of the QT interval in the electrocardiogram. Importantly, patients with protracted QT interval rate adaptation appear to have an increased arrhythmic risk [4], highlighting the importance of ventricular rate adaptation dynamics in arrhythmogenesis. A recent computational study based on *in vivo* human data has suggested a mechanism of reentry initiation from increased dispersion of APD adaptation in the presence of ischemia [5].

The aim of this study is to investigate the pro-arrhythmic effects of LV/RV differences in APD adaptation using simulations. Specifically, we aim to provide a quantitative characterization of the role of interventricular dispersion of repolarization in arrhythmogenesis, within a range of times and positions for the initiation of ectopicity. In order to achieve this, we develop a fast phenomenological model, able to reproduce the essential mechanisms involved in APD adaptation and the initiation of re-entry. Using an image-derived human ventricular model, we then compare two scenarios: one with normal difference in LV/RV adaptation, and another with slow, pathological, LV rate adaptation, leading to a larger dispersion in LV/RV repolarization. Below, the word "pathological" will be reserved for indicating the slow LV rate adaptation.

2. Methods

2.1. Anatomical Model

The anatomical model used for this study is a human ventricular mesh derived from computed tomography data [6], incorporating 55000 nodes. The model includes an algorithmically defined fibre orientation derived from experimental data [7], generated using the Chaste simulation package [8, 9]. As an aid for assigning specific properties to the respective ventricles, each node of the model

was given a value between 0 and 1, with values close to zero signifying LV specific properties and values close to 1 signifying specific RV properties. Additionally, simple description of a myocardial scar was incorporated manually by making the model non-conductive in an spherical volume centered around the septum, roughly mimicking an infarcted region resulting from LAD occlusion. Finally, a volume close to the scar, near the base of the RV, was assigned as the origin of ectopic beats. The anatomical model is shown in Fig. 1, along with color coding for the LV and RV properties, and the non-conductive and ectopic regions marked with the words SCAR and STIM respectively.

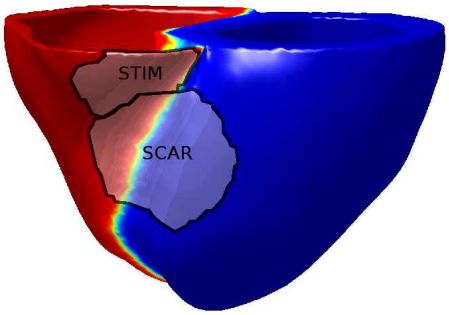

Figure 1. Computational anatomical model. Blue and red respectively signify LV and RV specific properties. The region marked SCAR is non-conductive, whereas STIM indicates the region of applied ectopic activity.

2.2. Conduction Model

To describe the electrical conduction properties of the model, we used the graph method developed in [10]. Briefly, the method relies on describing the cardiac tissue as a connected graph, where every edge is associated with a traveling cost. By finding the fastest path through the graph between pairs of nodes, activation times can be obtained with minimal computational cost. The costs $c_{i,j}$ associated with traveling along a graph edge connecting two nodes i and j are calculated according to

$$c_{i,j} = \sqrt{v(n_i, n_j)^T D_{i,j}^{-1} v(n_i, n_j)}/F, \qquad (1)$$

where $v(n_i, n_j)$ is the vector going from node i to node j, F is a speed function, and $D_{i,j}$ is a tensor describing the anisotropy resulting from the cell orientation between nodes i and j. The conduction paths in the model were computed using a modified version of Dijkstra's algorithm that will be described in Section 2.4.

2.3. Action Potential Model

The dynamics governing the adaptation of the action potential duration, A, within the model are described using the following recurrence relation for each node, following the approach presented in [11]:

$$A_{n+1} = [1 - \alpha\, e^{-D_n/\tau_2}]\, G(D_n) + [\alpha - 1 + \frac{A_n}{G(D_{n-1})}\, e^{-(A_n + D_n)/\tau_2)}]\, G(D_n), \qquad (2)$$

$$G(D_n) = a_1 - a_2\, e{-}D_n/\tau_1. \qquad (3)$$

Here, n is an index counting the number of action potential and D is the diastolic interval. The values for the parameters in Eqs. (2) and (3) were $a_{1,LV} = 404$, $a_{2,LV} = 197$, $\tau_{1,LV} = 77$, $\tau_{2,LV} = 76927$, $\alpha_{LV} = 1.05$ and $a_{1,RV} = 358$, $a_{2,RV} = 121$, $\tau_{1,RV} = 97$, $\tau_{2,RV} = 49399$ and $\alpha_{RV} = 1.08$ for LV and RV as indicated, and with $\tau_{2,LV} = 128720$ for the pathological, slower adaptation. These values were adapted to data presented in [5], using the Nelder-Mead optimization scheme as implemented in MATLAB. Figure 2 shows the dynamics of the APD dispersion resulting from the normal (solid line) and pathological adaptation properties (dashed line) respectively after a change of pacing interval from 750 ms to 400 ms.

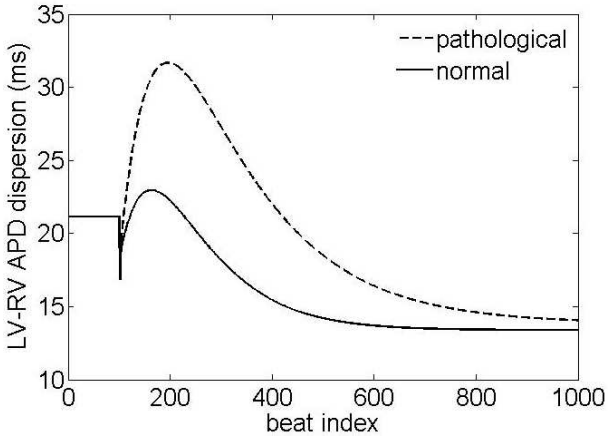

Figure 2. The figure shows the modelled LV/RV dispersion in APD after a change in pacing rate from 750 ms to 400 ms after 100 beats. Data is shown for the normal (solid line) and pathological (dashed line) case.

2.4. Activation and Repolarization Times

Based on the graph based method described in Section 2.2 and the model of APD adaptation described in Section 2.3, we now describe how the activation and repolarization at the tissue level are computed. The algorithm is similar to the well known Dijkstra's algorithm [12], but is modified to take repolarization into account, allowing nodes to be activated several times and thus allowing simulation of reentrant activation. This modification is roughly analogous to that presented for the fast marching method in [13].

Briefly, the algorithm works by using a priority queue Q to keep track of the order in which to expand nodes n to maintain a causal flow of information. In this context, expanding a node means finding its neighbours n_i, and calculating their arrival time $t(n_i)$, using information propagated from node n. The value of $t(n)$ is used to determine the position of a node n in Q. When a node is pulled from the queue, its APD is calculated according to Eq. (2). For a start node n_0, a pseudo-code description of the algorithm can be found in Algorithm 1.

Algorithm 1 Modified Dijkstra's Algorithm

$Q \leftarrow Q \cup n_0$
$t(n_0) \leftarrow 0$
while $Q \neq \emptyset$ **do**
$n \leftarrow argmin_{n \in Q} t(n)$
$Q \leftarrow Q \setminus n$
$APD(n) \leftarrow F(APD(n), DI_1(n), DI_0(n))$
$time \leftarrow t(n)$
for all $n_i \in NEIGHBOURS(n)$ **do**
if $t(n_i) + APD(n_i) < time + COST(n, n_i)$ **then**
$t(n_i) \leftarrow t(n) + COST(n, n_i)$
$Q \leftarrow Q \cup n_i$
end if
end for
end while

2.5. Initiation of Re-entry

The model was periodically activated from the bottom of both ventricles with a pacing interval of 750 ms until the APD distribution remained unchanged, followed by a change in pacing interval to 400 ms until the maximal dispersion in repolarization was reached after approximately 100 beats as shown in Fig. 2. Finally, reentry was initiated using an ectopic stimulus at the basal side of the non-conductive zone, inside the region marked STIM in Fig. 1.

Rather than keeping the timing and placement of the ectopic stimulus fixed, a range of different combinations within the STIM region were investigated. The times were varied between 265 ms and 295 ms in 10 steps, and 843 different positions were investigated, resulting in a set of 8430 possible combinations. This was done for both the normal and pathological adaptation parameters as described in Section 2.3, resulting in a total of 16860 simulated scenarios.

3. Results

Two sets of 8430 simulations were performed, corresponding to the normal and pathological LV APD adaptation, as described in the previous section. An individual simulation took of the order of 100 ms to compute, often leading to CPU times faster than realtime. For some combinations of position and timing of the ectopic beat, unidirectional block on the still-repolarizing LV side initiated a counter-clockwise reentry around the central conduction block as depicted in Fig. 3.

For each of the investigated timings of the ectopic stimulus, the percentage of positions within the STIM region of the ectopic stimulus that lead to re-entry was recorded. These results are visualized in Fig. 4. As can be seen from the figure, the pathological dispersion of repolarization lead to a marked increase in the probability of re-entry, as well as an extension of the range of timings of the ectopic beat which lead to re-entry. An ectopic beat at approximately 282 ms after last intrinsic activation appears to lead to the highest incidence of re-entry. At this time, the increased interventricular dispersion of repolarization lead to an approximately four-fold increase in the number of positions for the ectopic beat that lead to re-entry.

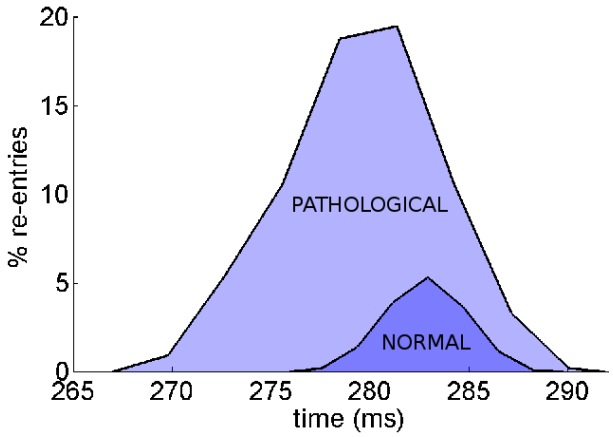

Figure 4. The figure shows the percentage of positions of the ectopic beat that lead to re-entry for each investigated timing. The upper curve corresponds to the pathological LV APD adaptation, while the lower curve corresponds to the normal LV APD adaptation.

4. Discussion

In this work, we have presented a method for simulating re-entry with minimal computational costs. The new method has enabled us to investigate the effects of interventricular dispersion of repolarization on the risk initiation of re-entry. In order to quantify the risk, a range of possible locations and timings were investigated, comprising a total of over 16000 simulated scenarios. This has allowed the quantification of the arrhythmic risk within the investigated range. Results show a marked increase in the probability of re-entry in the case of slow rate adaptation of the LV APD.

The employed graph based model provides a simplified

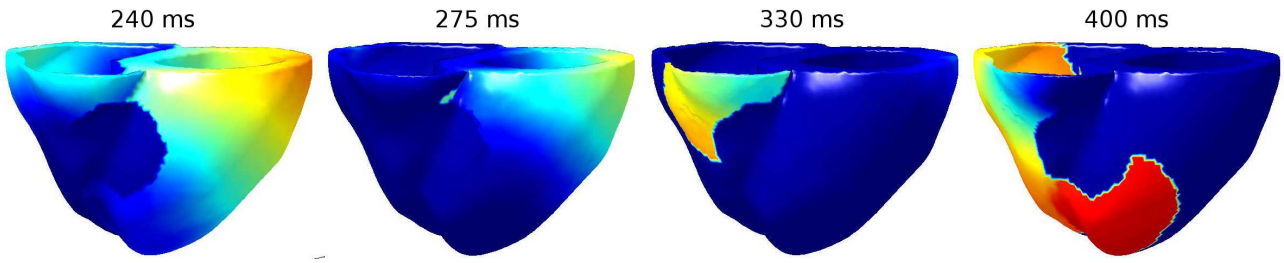

Figure 3. Electrical reentry following ectopic stimulation at 275 ms after last intrinsic activation. Unidirectional conduction block is caused by the slower APD adaptation of the LV, which is still repolarizing at the time of the ectopic stimulus. The four panels show the pseudo-potential of the tissue at 240, 275, 330 and 400 ms, for the left, middle left, middle right and right panels respectively.

representation of the dynamics properties of cardiac tissue. Although capturing essential characteristics of APD restitution and adaptation, it does not currently take into account effects from CV restitution and adaptation. The incorporation of such effects forms an interesting topic for future developments of the presented methods.

Acknowledgements

ABO was supported by Award No. KUK-C1-013-04, made by King Abdullah University of Science and Technology (KAUST). BR holds Medical Research Council Career Development, Industrial Partnership and Centenary Awards.

References

[1] Nash MP, Bradley CP, Sutton PM, Clayton RH, Kallis P, Hayward MP, Paterson DJ, Taggart P. Whole heart action potential duration restitution properties in cardiac patients: a combined clinical and modelling study. Experimental Physiology 2006;91(2):339–354.

[2] Kop WJ, Verdino RJ, Gottdiener JS, O'Leary ST, Bairey Merz CN, Krantz DS. Changes in heart rate and heart rate variability before ambulatory ischemic events(1). Journal of the American College of Cardiology 2001; 38(3):742–749.

[3] Eisenberg SJ, Scheinman MM, Dullet NK, Finkbeiner WE, Griffin JC, Eldar M, Franz MR, Gonzalez R, Kadish AH, Lesh MD. Sudden cardiac death and polymorphous ventricular tachycardia in patients with normal QT intervals and normal systolic cardiac function. The American journal of cardiology 1995;75(10):687–692.

[4] Pueyo E, Husti Z, Hornyik T, Baczk I, Laguna P, Varr A, Rodrguez B. Mechanisms of ventricular rate adaptation as a predictor of arrhythmic risk. American journal of physiology Heart and circulatory physiology 2010;298(5):H1577–1587.

[5] Bueno-Orovio A, Hanson BM, Gill JS, Taggart P, Rodriguez B. In vivo human left-to-right ventricular differences in rate adaptation transiently increase pro-arrhythmic risk following rate acceleration. PLoS ONE 2012; 7(12):e52234.

[6] Bernabeu M, Wallman M, Rodriguez B. Shock-induced arrhythmogenesis in a human model with patient-specific anatomy author. Heart Rhythm 2010;2010.

[7] Potse M, Dube B, Richer J, Vinet A, Gulrajani RM. A comparison of monodomain and bidomain reaction-diffusion models for action potential propagation in the human heart. IEEE Transactions on Biomedical Engineering 2006; 53(12):2425–2435.

[8] Bernabeu M, Bishop M, Pitt-Francis J, Gavaghan D, Grau V, Rodriguez B. High performance computer simulations for the study of biological function in 3D heart models incorporating fibre orientation and realistic geometry at paracellular resolution. In Computers in Cardiology, 2008. 2008; 721–724.

[9] Pitt-Francis J, Pathmanathan P, Bernabeu MO, Bordas R, Cooper J, Fletcher AG, Mirams GR, Murray P, Osborne JM, Walter A, et al. Chaste: a test-driven approach to software development for biological modelling. Computer Physics Communications 2009;180(12):2452–2471.

[10] Wallman M, Smith NP, Rodriguez B. A comparative study of graph-based, eikonal, and monodomain simulations for the estimation of cardiac activation times. IEEE transactions on bio medical engineering 2012;59(6):1739–1748.

[11] Kalb SS, Tolkacheva EG, Schaeffer DG, Gauthier DJ, Krassowska W. Restitution in mapping models with an arbitrary amount of memory. Chaos An Interdisciplinary Journal of Nonlinear Science 2005;15(2):023701. ISSN 10541500.

[12] Dijkstra EW. A note on two problems in connexion with graphs. Numerishe Mathematik 1959;1:269–271.

[13] Pernod E, Sermesant M, Konukoglu E, Relan J, Delingette H, Ayache N. A multi-front eikonal model of cardiac electrophysiology for interactive simulation of radio-frequency ablation. Computers textbackslash Graphics 2011;35:431–440.

Address for correspondence:

Mikael Wallman
Department of Computer Science, University of Oxford
Parks Rd, Oxford OX1 3QD, UK
mikw@cs.ox.ac.uk

RECENT REPORTS

13/06	A Volume-Based Method for Denoising on Curved Surfaces	Biddle von Glehn Macdonald März
13/07	Porous squeeze-film flow	Knox Wilson Duffy McKee
13/08	Diffusion of finite-size particles in confined geometries	Bruna Chapman
13/09	Mathematical analysis of a model for the growth of the bovine corpus luteum	Prokopiou Byrne Jeffrey Robinson Mann Owen
13/10	Capillary deformations of bendable films	Schroll Adda-Bedia Cerda Huang Menon Russell Toga Vella Davidovitch
13/11	Twist and stretch of helices: All you need is Love	Đuričković Goriely Maddocks
13/12	Switch on, switch off: stiction in nanoelectromechanical switches	Wagner Vella
13/13	Pinning, de-pinning and re-pinning of a slowly varying rivulet	Paterson Wilson Duffy
13/14	Travelling-wave similarity solutions for a steadily translating slender dry patch in a thin fluid film	Yatim Duffy Wilson
13/15	A stochastic model for early placental development	Cotter Klika Kimpton Collins Heazell
13/16	Experimentally-calibrated population of models predicts and explains inter-subject variability in cardiac cellular electrophysiology	Britton Bueno-Orovio Van Ammel Lu Towart Gallacher Rodriguez

13/23	Na/K pump regulation of cardiac repolarization: Insights from a systems biology approach	Bueno-Orovio Sánchez Pueyo Rodriguez
13/24	Cellular blebs - pressure-driven, axisymmetric, membrane protrusions	Woolley Gaffney Oliver Baker Waters Goriely
13/25	Growth-induced axial buckling of a slender elastic filament embedded in an isotropic elastic matrix	O'Keeffe Moulton Waters Goriely
13/26	The counterbend phenomenon: a generic property of the axoneme and cross-linked filament bundles	Gadêlha Gaffney Goriely
13/27	A well-posedness framework for inpainting based on coherence transport	März
13/28	Minimizing synchronizations in sparse iterative solvers for distributed supercomputers	Zhu Gu Liu

Copies of these, and any other OCCAM reports can be obtained from:

Oxford Centre for Collaborative Applied Mathematics
Mathematical Institute
24 - 29 St Giles'
Oxford
OX1 3LB
England
www.maths.ox.ac.uk/occam